Ferroelectric nature and real-space observations of domain motions in the organic charge-transfer compound tetrathiafulvalene-*p*-chloranil

Hideo Kishida,[1,2,3,*] Hisashi Takamatsu,[1] Ken Fujinuma,[1] and Hiroshi Okamoto[1,3]
[1]*Department of Advanced Materials Science, Graduate School of Frontier Sciences, University of Tokyo, 5-1-5 Kashiwanoha, Kashiwa, Chiba 277-8561, Japan*
[2]*Department of Applied Physics, Nagoya University, Furo-cho, Chikusa, Nagoya 464-8603, Japan*
[3]*CREST, Japan Science and Technology Agency (JST), Chiyoda-ku, Tokyo 102-0075, Japan*
(Received 31 July 2009; revised manuscript received 9 October 2009; published 6 November 2009)

Ferroelectricity in an organic charge-transfer compound, tetrathiafulvalene-*p*-chloranil (TTF-CA), originating from the one-dimensional valence and lattice instabilities, has been investigated by an electroreflectance (ER) method. Microscopic ER spectroscopy in the visible region enables real-space observations of both ferroelectric domain structures with a few hundred micrometers in size and depinning of the domain walls under strong electric fields. In addition, from ER spectroscopy in the infrared molecular-vibration region, we demonstrate that field-induced changes in the dimeric molecular displacement as well as charge transfer between TTF and CA molecules play an important role in the large dielectric response in TTF-CA.

DOI: 10.1103/PhysRevB.80.205201 PACS number(s): 78.40.Me, 78.20.Jq, 78.30.Jw, 77.84.Jd

I. INTRODUCTION

The realization of all-organic electronic devices requires organic ferroelectric components. At present, however, there are very few organic ferroelectric materials available. An exception is ferroelectric polymers wherein the unidirectional alignment of the built-in microscopic dipole moments is responsible for their ferroelectric properties. For a material to be ferroelectric, the centers for positive and negative charges in the material must be spatially separate. In an organic charge-transfer (CT) compound, charge transfer between electron donating molecules (donor: D) and electron accepting molecules (acceptor: A) can be a possible candidate for the separation of positive- and negative-charge centers leading to ferroelectricity. A prototypical example of such CT compounds is tetrathiafulvalene-*p*-chloranil (TTF-CA).

TTF-CA has been attracting significant recent attention because of other exotic phenomena, for example, neutral(N)-ionic(I) valence phase transition[1–7] and its photocontrol.[8–16] In TTF-CA, the D molecules of TTF and the A molecules of CA [Fig. 1(a)] are alternately stacked and form one-dimensional (1D) chains. These stacks are three-dimensionally arranged to form a three-dimensional (3D) crystal. At room temperature, TTF-CA is in the N phase and is regarded as a van der Waals crystal. By lowering the temperature, it undergoes phase transition from the N phase to the I phase at 81 K.[1,2,17,18] Because of the CT interaction between neighboring D and A molecules, the degree of CT (ρ) between TTF and CA, denoted as $TTF^{+\rho}$ and $CA^{-\rho}$, is not equal to 0 or 1 but rather is ~0.3 in the N phase and ~0.7 in the I phase.[2,3,18–21] The I phase in TTF-CA is stabilized by the energy gain due to long-range Coulombic attractive interaction (the Madelung potential), which is enhanced by the shrinking of the lattice constants with the decrease in the temperature.[22]

Another important feature of the NI transition in TTF-CA is that, in the I phase, the DA molecules are dimerized to form spin-singlet states. While such molecular dimerization has been explained mainly by the spin-Peierls (SP) mechanism,[14] the effect of the long-range Coulomb interactions is also theoretically discussed.[23,24] It is known that most of the ionic CT compounds show the molecular dimerization at low temperature due to this mechanism. The detailed structural studies have revealed that the dimeric molecular displacements exhibit three-dimensional in-phase order, leading to ferroelectric nature.[22,25,26] This three-dimensional order suggests that the interchain electrostatic interaction is important for the dimerizations as well as the SP mechanism. Thus, we can consider that the ferroelectricity in TTF-CA originates from the cooperation of the valence instability of DA molecules, the SP mechanism, and the ferroelectric interchain interaction.[27,28] For example, a change in ρ will modify the spin state of each molecule and then it may give rise to the change in the molecular displacements through the spin-lattice interaction. Such couplings among charge, spin, and lattice degrees of freedom suggest that TTF-CA should show ferroelectric behavior different from that observed in conventional displacive-type or order-disorder-type ferroelectricity.[29]

The ferroelectric nature in TTF-CA can be revealed by measurement of the optical spectra under electric field.[17,30,31] In the previous proceeding papers,[30,31] we partially discussed

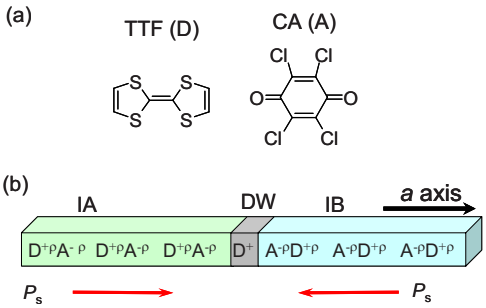

FIG. 1. (Color online) Structures of TTF-CA. (a) Chemical structure of TTF and CA. (b) Schematic of the ionic chain structure of TTF-CA. The DW is located between the rightward polarized domain (IA) and the leftward one (IB). The spontaneous polarization, P_s, is directed in opposite directions in the IA and IB domains.

the electroreflectance (ER) spectra of TTF-CA and reported that the sign of the ER signals can give information of the polarization of ferroelectric domains. The present study is the extended version of the previous studies; by observing the static domain structures and their dynamics under high electric field, we clarify the detailed ferroelectric nature of TTF-CA. In addition, by measuring ER spectra for the intramolecular vibrational modes, we quantitatively discuss the electric-field-induced changes in the degree of charge transfer and the molecular dimerizations.

II. EXPERIMENTAL PROCEDURES

Single crystals of TTF-CA were obtained by cosublimation of two constituent molecules. The component molecules were purified by recrystallization and sublimation procedures. The electrodes are made of carbon paste and painted on the surface of the crystal.

To unravel the ferroelectric nature and related charge and lattice dynamics in TTF-CA, we applied the ER spectroscopy using single-crystal samples in both the visible and IR regions and observed changes in the reflectance spectra induced by the applied electric field. In this study, we performed ER measurements using three configurations. The first configuration was macroscopic ER in the visible region, in which the spot size of light for measurements was about 500 μm in diameter, the amplitude of the alternating electric field was 0.25–10 kV/cm, and the frequency was 1 kHz. The second configuration used was microscopic ER in the visible regions in which the ER signals were detected using specially designed microscope-equipped spectrometers. In the above two experiments, the electric-field-induced change in the reflectivity, ΔR, was detected using the lock-in method. When we apply an alternating electric field, $F=F_0 \cos \omega t$, ΔR can be written as follows:

$$\Delta R(F) = R'(0)F_0 \cos \omega t + (1/2)R''(0)(F_0)^2(1+\cos 2\omega t)/2 + \cdots . \quad (1)$$

The first term appears only in the case when the inversion symmetry is broken. By the choice of the frequency (ω or 2ω) in the lock-in method, we can detect the signals for the first and the second terms separately, which are called the $1f$ and the $2f$ signals, respectively, in the following discussion. Finally, the third configuration was ER measurement in the IR region, in which we used a Fourier-transform (FT)-IR spectrometer.

In the ER measurements using FT-IR, we applied a static electric field to the sample. The polarity of the electric field is switched by the sequence, zero-positive-zero-negative-zero, to imitate the alternating field. $\Delta R/R$ is obtained from the following relation:

$$\Delta R/R = [(R_+ - R_0) + (R_- - R_0)]/R_0. \quad (2)$$

Here, R_+, and R_- are the reflectivities for the positive and the negative electric fields, respectively. R_0 is the reflectivity at zero field. The obtained spectrum corresponds to the $2f$ component in the lock-in method. $1f$ signals are also observed (not shown in this paper) and yield similar information as the $2f$ signals. However, the $1f$ signal has an ambiguity of sign depending on the direction of ferroelectric polarization. Therefore, we have only discussed the $2f$ signals for FT-IR ER measurements.

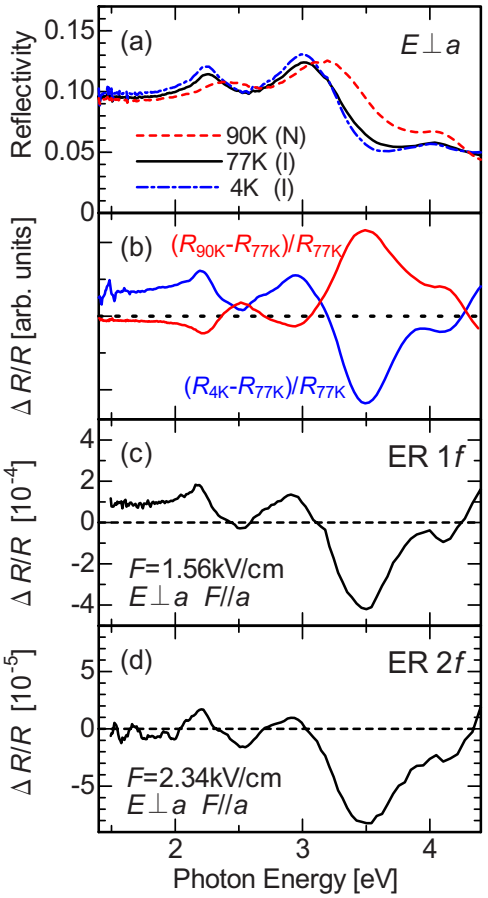

FIG. 2. (Color online) Reflectivity and electroreflectance spectra of TTF-CA. (a) Reflectivity (R) spectra of TTF-CA at 4 K (dashed-dotted line), 77 K (solid line), and 90 K (dashed line). (b) Difference spectra of reflectivity ($\Delta R/R$) with a change in temperature from 77 to 4 K $[(R_{4\ \mathrm{K}}-R_{77\ \mathrm{K}})/R_{77\ \mathrm{K}}]$ and from 77 to 90 K $[(R_{90\ \mathrm{K}}-R_{77\ \mathrm{K}})/R_{77\ \mathrm{K}}]$. (c) $1f$ component of the ER spectrum of TTF-CA (77 K). (d) $2f$ component of the ER spectrum of TTF-CA (77 K). In the measurements of the $1f$ and $2f$ components, the polarization of light, E, is perpendicular to the one-dimensional axis ***a***, and the applied electric field, F, is parallel to the a axis. The reflectivity spectra for 4 and 77 K and ER spectra are presented in Ref. 30.

III. RESULTS AND DISCUSSIONS

A. Reflectivity spectra of TTF-CA

The reflectivity (R) spectra of TTF-CA from 1.4 to 4.4 eV at 90 K (N phase), 77 K (I phase) and 4 K (I phase) are shown in Fig. 2(a) for polarization perpendicular to the DA stacking axis (the **a** axis), which is almost parallel to the molecular plane. The peaks around 2.25 and 3 eV were attributed to the intramolecular transitions in TTF,[3] the energies of which are known to shift sensitively depending on ρ. By lowering the temperature, the peaks shift to lower

energies due to an increase in ρ. The values of ρ evaluated from the frequency of the IR C=O stretching mode of CA, which is a more quantitative probe for ρ are 0.32 (90 K), 0.53 (77 K), and 0.59 (4 K).[19] The difference reflectivity spectra $(R_{4\ \mathrm{K}}-R_{77\ \mathrm{K}})/R_{77\ \mathrm{K}}$ between 77 $(R_{77\ \mathrm{K}})$ and 4 K $(R_{4\ \mathrm{K}})$ and $(R_{90\ \mathrm{K}}-R_{77\ \mathrm{K}})/R_{77\ \mathrm{K}}$ between 77 and 90 K $(R_{90\ \mathrm{K}})$ are shown in Fig. 2(b). For the spectrum of $(R_{4\ \mathrm{K}}-R_{77\ \mathrm{K}})/R_{77\ \mathrm{K}}$, there are two positive peaks around 2.25 and 3.0 eV and a sharp dip around 3.5 eV. The spectral shape of $(R_{90\ \mathrm{K}}-R_{77\ \mathrm{K}})/R_{77\ \mathrm{K}}$ is similar to that of $(R_{4\ \mathrm{K}}-R_{77\ \mathrm{K}})/R_{77\ \mathrm{K}}$, except for the sign. The $(R_{4\ \mathrm{K}}-R_{77\ \mathrm{K}})/R_{77\ \mathrm{K}}$ and $(R_{90\ \mathrm{K}}-R_{77\ \mathrm{K}})/R_{77\ \mathrm{K}}$ spectra correspond to the reflectivity change due to the increase and decrease in ρ from the value at 77 K, respectively. Thus, changes in the reflectivity peaks in the visible region can be a good measure for changes in ρ.

B. Macroscopic ER measurements

The $1f$ and $2f$ spectra obtained by macroscopic ER measurements at 77 K are shown in Figs. 2(c) and 2(d), respectively. The spectral shapes of the $1f$ and $2f$ components are both coincident with the $(R_{4\ \mathrm{K}}-R_{77\ \mathrm{K}})/R_{77\ \mathrm{K}}$ spectrum. It should be noted that the sign of the $1f$ signal is dependent on the samples and also on the measured positions in a crystal while its spectral shape is unchanged. On the other hand, the sign of the $2f$ signal is always unchanged and is the same as the sign of $(R_{4\ \mathrm{K}}-R_{77\ \mathrm{K}})/R_{77\ \mathrm{K}}$. This suggests that the $2f$ measurement detects the increase in ρ by the electric field.

The emergence of the $1f$ signal indicates that inversion symmetry is lost in the measured area and therefore the ferroelectric domain has macroscopic scale. The position dependence of the sign of the $1f$ signal makes us expect that ferroelectric domains with opposite polarizations, schematically illustrated in Fig. 1(b) as IA and IB, coexist in a crystal. In IA (IB), a D molecule moves to right (left) and an A molecule moves to the left (right), leading to a dipole moment (P_s) with the right (left) direction. Thus, there is a spontaneous dipole moment in each area. The difference in sizes of the IA and IB domains is the reason why $1f$ signals are observed in the macroscopic ER measurements. Here, we assume that the sizes of IA and IB domains are unchanged by the electric field. Namely, we assume that the domain wall (DW) between the IA and the IB domains[32–35] cannot move. Even in such a case, changes in a spontaneous dipole moment can be detected in the $1f$ signal. The magnitude of the dipole moment in a domain is proportional to the product of ρ and the dimeric molecular displacement (δ), both of which may be changed by the electric field. Since the present ER measurement probes the change in ρ the dielectric response in a ferroelectric domain can be observed as a change in ρ. The change in P_s and ρ by the electric field is schematically illustrated in Fig. 3(a), in which the IA and IB domains are shown as 1D stacks for simplicity. The contribution of the field-induced change in δ will be discussed later.

When a DW moves due to the electric field, the number of molecules (N_A and N_B) in each domain is changed and thus different dielectric responses will be observed. It should be noted that the DW motion induced by the electric field (or equivalently the field-induced changes in N_A and N_B) contributes not to the $1f$ component but to the $2f$ component. The sign of the $2f$ signal obtained experimentally is independent of the samples, indicating that the electric field enhances ρ irrespective of the direction of the electric field, in contrast to the case of the $1f$ signal. It has been theoretically predicted that an effective charge exists on a DW; the D-molecule-centered DW is positively charged and the A-molecule-centered DW is negatively charged.[36] When the electric field drives the motion of the DW, the ratio of the IA and IB domains changes depending on the direction of the electric field, as illustrated in Fig. 3(b); the IA domain is expanded (shrunk) for the right (left) direction of the electric field. As a result, the electric field should also result in an increase in ρ averaged over the whole crystal, irrespective of the direction of the electric field. Such increases in ρ yield $2f$ signals as observed in the ER measurements. The changes in P_s and ρ responsible for the $2f$ signals are schematically illustrated in Fig. 3(b).

The dependence of the $1f$ and $2f$ signals on the amplitude of the electric field is shown in Fig. 4(a). The magnitude of

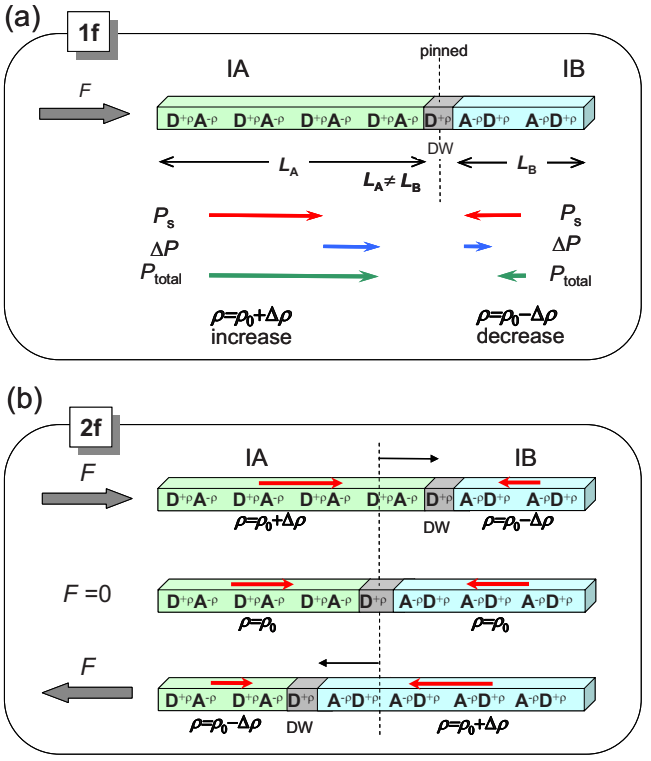

FIG. 3. (Color online) The mechanism of the origin of ER signals in TTF-CA. (a) The mechanism of the $1f$ signal. The lengths of IA and IB domains, L_A and L_B, are not balanced. The direction of spontaneous polarizations, P_s, in IA and IB are opposite, while the electric-field-induced polarizations, ΔP, in IA and IB are parallel. Consequently, the polarizations are enhanced and reduced in IA and IB, respectively. These changes in the polarization are accounted for by the changes in ρ. (b) The mechanism of the $2f$ signal. The rightward applied electric field [upper row in Fig. 3(b)] moves the DW rightward from the point at $F=0$ (middle). In the dominant domain (IA), ρ is increased. The leftward field (lower) moves the DW leftward. In the dominant domain (IB), ρ is increased again. In a single cycle of the applied electric field, ρ is increased twice.

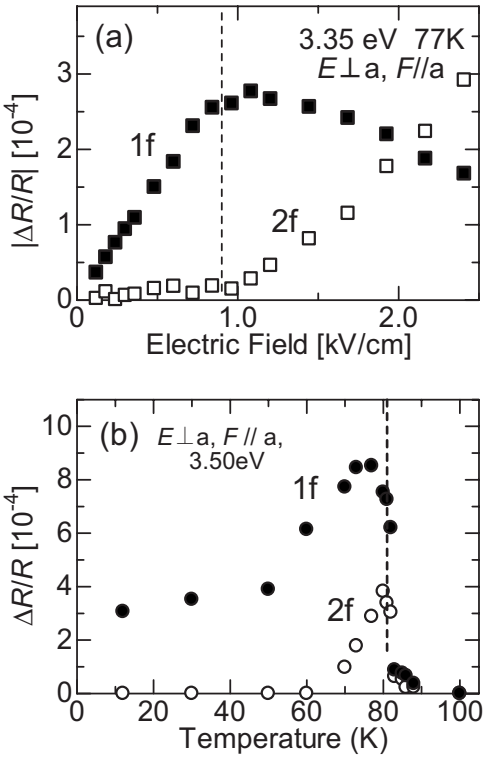

FIG. 4. (a) Electric-field dependence of ER signals (filled squares: $1f$, open squares: $2f$) measured at 3.35 eV. (b) Temperature dependence of $1f$ and $2f$ ER signals between 12 and 100 K with $F=1.56$ kV/cm ($1f$) and 2.34 kV/cm ($2f$).

the $1f$ signal can be detected at levels as low as 0.15 kV/cm and is almost proportional to the electric field up to 0.9 kV/cm. The $1f$ signal is purely due to the electronic response. It is therefore reasonable to assume that the onset electric field is nearly equal to zero. On the other hand, the $2f$ signal was never detected below a threshold value ($F_{\mathrm{th}} \sim 0.9$ kV/cm). The $2f$ signal originates in the electric-field-induced DW motion. Since DWs have charges as mentioned above, it is natural to consider that they are pinned and can be moved only by a strong electric field.

The temperature dependence of ER signals with $F=1.56$ kV/cm ($1f$) and 2.34 kV/cm ($2f$) is shown in Fig. 4(b). The $1f$ signals can be observed at the whole temperature range below T_c. On the other hand, the $2f$ signals can be observed only just below T_c. Below 60 K, no $2f$ signals are observed. Since the $1f$ signal results mainly from the electronic response, it is natural that the $1f$ signal is observed even at 10 K which is much lower than T_c. The $2f$ signals are related to the motion of DWs and the pining of DWs can be easily released near T_c. Therefore, it is reasonable that the $2f$ signal is enhanced with increase in temperature to T_c. Thus, our assignments of the origins of each signal explain well the temperature dependence of ER signals.

C. Microscopic ER measurements

To obtain detailed information on the spatial distribution of the ferroelectric domains and their field-induced changes, we performed ER measurements under a microscope. The probe light was shaped as a 27 μm$\times$27 μm square. We observed ER signals at 225 points on a crystal surface with a size of 400 μm$\times$400 μm. The signs of the $1f$ signals were found to change depending on the positions. The typical $1f$ spectra with opposite signs in a crystal, which was measured with $F=2$ kV/cm (the low electric-field regime), are shown in Fig. 5(a). The data of the $1f$ signals measured at 3.5 eV are mapped in Fig. 5(b), in which the signal intensity is plotted after two-dimensional numerical smoothing. As shown in the figure, the positive and the negative areas (the areas of the IA and IB domains) are spatially separated and form macroscopic ferroelectric domains. The domains are not one dimensional and their typical dimension is a few hundred microns. The boundaries between IA and IB domains correspond to the DWs. The observed domain pattern under a low electric field did not change during the measurements.

By comparison of the microscopically measured $\Delta R/R$ with $(R_{4\ \mathrm{K}}-R_{77\ \mathrm{K}})/R_{77\ \mathrm{K}}$, we calculated the magnitude of the modulation $\Delta\rho$ of ρ to be $\Delta\rho=5.7\times10^{-4}$. In this calculation, we assumed that the measured single area is completely polarized to one direction. In a whole crystal, the

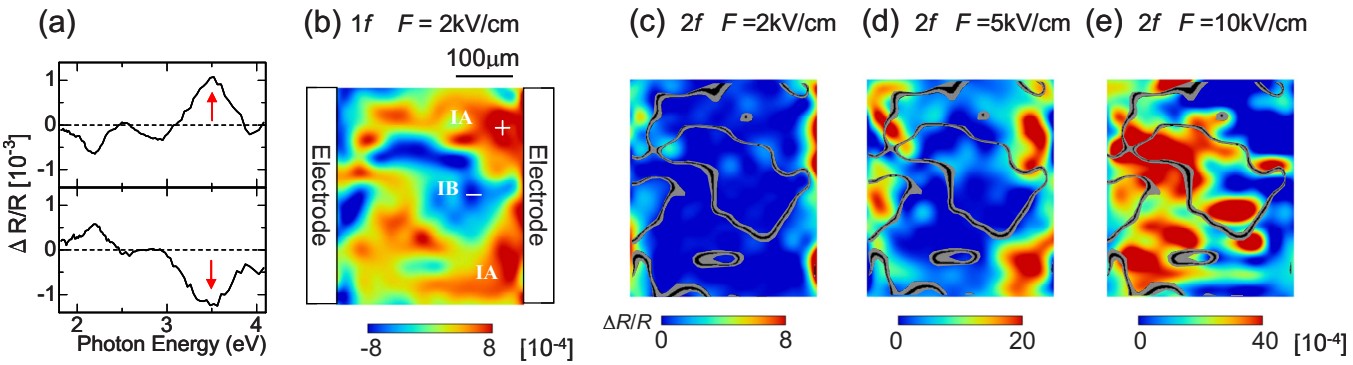

FIG. 5. (Color online) (a) Typical $1f$ spectra at the measured points in the IA (upper panel) and IB (lower) domains. The measured photon energy in the mapping measurement is indicated by arrows. (b) The map of the $1f$ signals obtained by two-dimensional smoothing of the raw data. The measuring points of the spectra shown in Fig. 5(a) are shown in Fig. 5(c) with + and − symbols. [(c), (d), and (e)] The maps of the $2f$ signals measured at (c) 2 kV/cm, (d) 5 kV/cm, and (e) 10 kV/cm. The black and gray area in (e) indicates the domain boundary between IA and IB, obtained from the $1f$ measurements.

sizes of IA and IB are different. The absolute value of the signal in the macroscopic measurement shown in Fig. 3(c) is therefore smaller than that in the microscopic one shown in Fig. 5(a).

The similar maps for the $2f$ signals obtained at 3.5 eV are shown in Figs. 5(c)–5(e) for the electric-field range of 2–10 kV/cm. At 2 kV/cm, the $2f$ signals appear only near the electrodes [Fig. 5(c)]. With increasing electric field, the area in which the $2f$ signal could be observed over the wider region [Fig. 5(d)]. At 10 kV/cm, the $2f$ signals were observed over nearly the whole area [Fig. 5(e)]. In Fig. 5(e), the positions of the DWs between the IA and IB domains, which correspond to the zero-signal points in Fig. 5(b), are shown by the black and gray lines, which seem to be correlated with the areas in which the $2f$ signals could be detected.

As seen in Fig. 5(e), at 10 kV/cm, the DWs can move over a wide spatial region. More interestingly, at higher fields, above 10 kV/cm, electric switching to a low-resistivity state was observed. At the critical field (F_c), the electric conductivity showed a sudden jump (not shown). This switching phenomenon has been previously reported[37] and the magnitude of F_c is consistent with that of the reported value. Taking into account the DW dynamics shown in Figs. 5(c)–5(e), the switching phenomenon at the high field can be explained in the following way. At around 0.9 kV/cm, the DWs start to move. At around 10 kV/cm, pinnings of the DWs become very weak. Since the DWs move collectively, as seen in Fig. 5(e), the ferroelectric domain structure was preserved. This three-dimensional nature of domains and DWs' motions indicates that the electrostatic interchain interaction is important in the dimerization mechanism. Above 10 kV/cm, the 3D pinning of DWs completely disappear and the DWs can move almost freely. In this case, the DWs are one dimensional in nature, resulting in the crystal becoming highly conductive, as reported previously.

D. IR ER measurements under electric field

The ER signals in the visible regions are all ascribed to the modulation effect to the degree of CT (ρ), namely, the charge part. Considering that the charge and the lattice are strongly coupled in this type of CT compounds, it is plausible that the electric field modulates not only the charge part but also the lattice part (or equivalently the molecular displacements) via the spin-Peierls instability. In order to detect these two contributions separately, we performed ER measurements for the phonon modes. It has been established that ρ can be quantified by the frequency of the b_{1u} C=O stretching mode of CA molecules.[2] This mode is located around 1681 cm^{-1} in the neutral CA molecule while it is located around 1518 cm^{-1} in the ionic CA molecule and the frequency of the mode is linearly dependent on ρ. This behavior is well explained by the fact that the antibonding character of the added electron on the C=O bond results in the increase in the C=O bond lengths.[38] On the other hand, the degree of dimerization is reflected by the IR intensity of the intramolecular vibrations with a_g symmetry (the a_g modes). Though the molecular a_g modes are optically forbidden, the dimerization of DA molecules along the 1D stacks, which leads to breakdown of the inversion symmetry, makes the molecular a_g mode IR active, because the intramolecular a_g mode couples with the CT transition along the 1D stack. The absorption intensity of the mode is almost proportional to the magnitude of the dimerization[2,17] so that the a_g mode can be used as a good probe of the dimerization. Thus, the degree of CT and the dimerization can be probed by the IR absorptions.

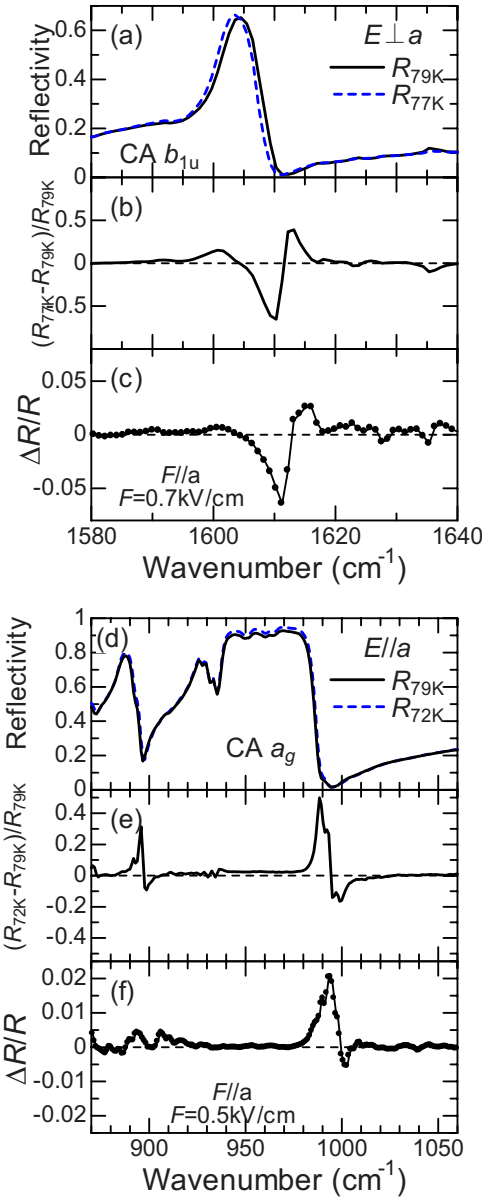

FIG. 6. (Color online) Infrared reflectivity spectra perpendicular and parallel to the one-dimensional axis, corresponding to the b_{1u} C=O stretching mode of CA (a) and a_g C-Cl stretching modes of CA (d) measured at 79 K. In (b) and (e), the difference spectra of the reflectivity spectra with decreasing temperature are shown. In (c) and (f), the $2f$-component ER spectra ($\Delta R/R$) are shown.

In Fig. 6(a), the reflectivity spectra ($E \perp a$) for the b_{1u} C=O stretching mode of CA at 77 and 79 K are presented, and the difference spectrum between 77 and 79 K, $(R_{77\ K} - R_{79\ K})/R_{79\ K}$, is shown in Fig. 6(b). The frequency of the mode decreases with decreasing temperature due to the in-

crease in ρ. The $2f$ component of the ER spectrum with $F=0.7$ kV/cm is shown in Fig. 6(c), the spectral shape of which is very similar to $(R_{77\ \mathrm{K}}-R_{79\ \mathrm{K}})/R_{79\ \mathrm{K}}$. This shows the field-induced increase in the averaged ρ The mechanism for this $2f$ component is similar to that in the visible regions, namely, the motions of the DWs expand the domains polarized parallel to the electric field, and the averaged ρ is increased through the increase in ρ in the dominant domains. The change in ρ, $\Delta\rho/\rho$, is $\approx 0.08\%$ at $F=0.7$ kV/cm.[39]

In Fig. 6(d), the reflectivity spectra $(E\|a)$ for the a_g modes of CA at 72 and 79 K are presented, together with the difference spectrum between 72 and 79 K, $(R_{72\ \mathrm{K}}-R_{79\ \mathrm{K}})/R_{79\ \mathrm{K}}$, in Fig. 6(e). The high reflection band at around 950 cm^{-1} is due to the a_g C-Cl stretching mode of CA.[38] With decreasing temperature, this band is broadened, suggesting an increase in the intensity due to enhancement of the dimerization. The ER spectrum for the a_g mode is shown in Fig. 6(f), which is again very similar to the difference spectrum in Fig. 6(e). Therefore, we can conclude that the dimeric molecular displacement, δ is increased by the electric field. The original magnitude of the dimerization defined as $2\delta/L$ (L: the lattice constant along the **a** axis) is 0.025,[22] and the change in the displacement $\Delta\delta/\delta$ is $\approx 0.04\%$ at $F=0.5$ kV/cm, which is comparable with $\Delta\rho/\rho$. The observed field-induced increase in δ is attributable to the enhancement of the effective electron (spin)-lattice coupling by the increase in the spin density in each molecule, which originates from the field-induced increase in ρ. Thus, by using IR spectroscopy under an electric field, we could clearly demonstrate that the electric field modulates not only the degree of CT but also the degree of lattice dimerization. This result provides unambiguous direct evidence for the strong spin-lattice coupling in TTF-CA.

IV. CONCLUSION

In conclusion, we studied the ferroelectric mechanism of the organic charge-transfer compound, TTF-CA, by electroreflectance measurements in both visible and IR regions. The macroscopic electroreflectance measurement revealed that the electric field induces charge transfer between the dimerized TTF and CA pair. This is the microscopic origin of the dielectric response. By mapping the electroreflectance signals using optical microscopy, we succeeded in visualizing ferroelectric domains with a few hundreds of μm in size and were able to show that domain walls between oppositely polarized ferroelectric domains exist. At a low electric field, the domain walls are pinned, while at a higher electric field, the pinning is released and the domain walls can be driven by the electric field. Moreover, by electroreflectance measurements in the IR region, we demonstrated that the electric field modulates not only the degree of charge transfer but also the molecular dimerization via the strong electron (spin)-lattice coupling. The electroreflectance spectroscopy presented here should be a powerful tool for the clarification of microscopic physical mechanism of ferroelectricity as well as for the observation of real-space images of ferroelectric domains.

ACKNOWLEDGMENTS

This work was supported in part by MEXT (Grants No. 16654049, No. 18684014, No. 16076207, and No. 20110005).

*kishida@nuap.nagoya-u.ac.jp

[1] J. B. Torrance, J. E. Vazquez, J. J. Mayerle, and V. Y. Lee, Phys. Rev. Lett. **46**, 253 (1981).
[2] A. Girlando, F. Marzola, C. Pecile, and J. B. Torrance, J. Chem. Phys. **79**, 1075 (1983).
[3] Y. Tokura, T. Koda, G. Saito, and T. Mitani, J. Phys. Soc. Jpn. **53**, 4445 (1984).
[4] M. H. Lemée-Cailleau, M. Le Cointe, H. Cailleau, T. Luty, F. Moussa, J. Roos, D. Brinkmann, B. Toudic, C. Ayache, and N. Karl, Phys. Rev. Lett. **79**, 1690 (1997).
[5] V. Oison, C. Katan, P. Rabiller, M. Souhassou, and C. Koenig, Phys. Rev. B **67**, 035120 (2003).
[6] T. Iizuka-Sakano, T. Kawamoto, Y. Shimoi, and S. Abe, Phys. Rev. B **70**, 085111 (2004).
[7] M. Buron-LeCointe, M. H. Lemée-Cailleau, H. Cailleau, S. Ravy, J. F. Bérar, S. Rouzière, E. Elkaïm, and E. Collet, Phys. Rev. Lett. **96**, 205503 (2006).
[8] S. Koshihara, Y. Tokura, T. Mitani, G. Saito, and T. Koda, Phys. Rev. B **42**, 6853 (1990).
[9] T. Suzuki, T. Sakamaki, K. Tanimura, S. Koshihara, and Y. Tokura, Phys. Rev. B **60**, 6191 (1999).
[10] S. Koshihara, Y. Takahashi, H. Sakai, Y. Tokura, and T. Luty, J. Phys. Chem. B **103**, 2592 (1999).
[11] S. Iwai, S. Tanaka, K. Fujinuma, H. Kishida, H. Okamoto, and Y. Tokura, Phys. Rev. Lett. **88**, 057402 (2002).
[12] T. Luty, H. Cailleau, S. Koshihara, E. Collet, M. Takesada, M. H. Lemée-Cailleau, M. Buron-Le Cointe, N. Nagaosa, Y. Tokura, E. Zienkiewicz, and B. Ouladdiaf, Europhys. Lett. **59**, 619 (2002).
[13] E. Collet, L. Guerin, N. Uchida, S. Fukaya, H. Shimoda, T. Ishikawa, K. Matsuda, T. Hasegawa, A. Ota, H. Yamochi, G. Saito, R. Tazaki, S. Adachi, and S. Koshihara, Science **300**, 612 (2003).
[14] H. Okamoto, Y. Ishige, S. Tanaka, H. Kishida, S. Iwai, and Y. Tokura, Phys. Rev. B **70**, 165202 (2004).
[15] S. Iwai, Y. Ishige, S. Tanaka, Y. Okimoto, Y. Tokura, and H. Okamoto, Phys. Rev. Lett. **96**, 057403 (2006).
[16] K. Yonemitsu and K. Nasu, Phys. Rep. **465**, 1 (2008).
[17] Y. Tokura, Y. Kaneko, H. Okamoto, S. Tanuma, T. Koda, T. Mitani, and G. Saito, Mol. Cryst. Liq. Cryst. **125**, 71 (1985).
[18] Y. Tokura, T. Koda, T. Mitani, and G. Saito, Solid State Commun. **43**, 757 (1982).
[19] S. Horiuchi, Y. Okimoto, R. Kumai, and Y. Tokura, J. Phys. Soc. Jpn. **69**, 1302 (2000).
[20] S. Horiuchi, Y. Okimoto, R. Kumai, and Y. Tokura, Science **299**, 229 (2003).
[21] M. Masino, A. S. Girlando, and Z. G. Soos, Chem. Phys. Lett. **369**, 428 (2003).
[22] M. Le Cointe, M. H. Lemée-Cailleau, H. Cailleau, B. Toudic, L.

Toupet, G. Heger, F. Moussa, P. Schweiss, K. H. Kraft, and N. Karl, Phys. Rev. B **51**, 3374 (1995).
[23] T. Iizuka-Sakano and Y. Toyozawa, J. Phys. Soc. Jpn. **65**, 671 (1996).
[24] P. Huai, H. Zheng, and K. Nasu, J. Phys. Soc. Jpn. **69**, 1788 (2000).
[25] Y. Kanai, M. Tani, S. Kagoshima, Y. Tokura, and T. Koda, Synth. Met. **10**, 157 (1984).
[26] P. García, S. Dahaoui, C. Katan, M. Souhassou, and C. Lecomte, Faraday Discuss. **135**, 217 (2007).
[27] H. Okamoto, T. Mitani, Y. Tokura, S. Koshihara, T. Komatsu, Y. Iwasa, T. Koda, and G. Saito, Phys. Rev. B **43**, 8224 (1991).
[28] J. I. Kishine, T. Luty, and K. Yonemitsu, Phys. Rev. B **69**, 075115 (2004).
[29] Z. G. Soos, S. A. Bewick, A. Peri, and A. Painelli, J. Chem. Phys. **120**, 6712 (2004).
[30] H. Kishida, K. Fujinuma, and H. Okamoto, Synth. Met. **120**, 909 (2001).
[31] H. Kishida, K. Fujinuma, H. Takamatsu, and H. Okamoto, Trans. Mater. Res. Soc. Jpn. **30**, 75 (2005).
[32] T. Mitani, G. Saito, Y. Tokura, and T. Koda, Phys. Rev. Lett. **53**, 842 (1984).
[33] Y. Okimoto, S. Horiuchi, E. Saitoh, R. Kumai, and Y. Tokura, Phys. Rev. Lett. **87**, 187401 (2001).
[34] S. A. Bewick and Z. G. Soos, Chem. Phys. **325**, 60 (2006).
[35] Z. G. Soos and A. Painelli, Phys. Rev. B **75**, 155119 (2007).
[36] N. Nagaosa, J. Phys. Soc. Jpn. **55**, 2754 (1986).
[37] Y. Tokura, H. Okamoto, T. Koda, T. Mitani, and G. Saito, Phys. Rev. B **38**, 2215 (1988).
[38] C. Katan, P. E. Blöchl, P. Margl, and C. Koenig, Phys. Rev. B **53**, 12112 (1996).
[39] In the IR ER measurements, we obtained detectable $2f$ signals at 0.5–0.7 kV/cm. At such low electric field, we do not observe any $2f$ signal in the macroscopic ER measurements because the magnitude of the electric field is below the threshold of depinning of domain walls. In the IR ER measurements, we alternate the direction of the dc electric field every 25 seconds and imitate the ac field while we applied 1 kHz ac electric field in the macroscopic ER experiments. This difference of frequency leads to the lowering of the threshold of $2f$ signals in the IR ER measurements.